# 27

# Human Neural Network Dynamics Using Multimodal Registration of EEG, PET, and MRI

**Robert W. Thatcher, *,† Camilo Toro,* Mark E. Pflieger,‡ and Mark Hallett***

**Medical Neurology Branch, Clinical Neuroscience Program, National Institutes of Neurological Disorders and Stroke, National Institutes of Health, Bethesda, Maryland 20892; and ‡Neuroscan, Inc., El Paso, Texas 79902*

## I. Introduction

Recent studies report zero phase locking of coherent multiunit activity during perceptual and motor tasks (Gray *et al.*, 1989; Eckhorn *et al.*, 1988; Murthy and Fetz, 1992). These studies and others (Atiya and Baldi, 1989; John, 1963; Thatcher and John, 1977) have hypothesized that the temporal characteristics of pools of oscillating neurons are used to encode information and to label various features of an object by phase-locked and coherent activity of the corresponding feature extracting neurons. Specifically, phase locking serves to link associated features in different neural systems to form a coherency of spatially organized phase and frequency relationships within and between neural networks (Grossberg, 1976; Grossberg and Somers, 1991; von der Malsburg and Schneider, 1986; Baldi and Meir, 1990).

Similar properties of phase locking and coherency between distributed neural networks have been reported by Gevins and colleagues in visual–spatial tasks using scalp-recorded EEG and evoked potential analyses in humans (Gevins *et al.*, 1989a, 1989b; Gevins and Bressler, 1988). Phase locking and coherency between scalp-recorded EEG was also recently observed in a human voluntary motor movement task using measures of instantaneous EEG coherence and phase (Thatcher *et al.*, 1993a, 1993b). The latter study showed rapid increases and decreases in the magnitude of EEG coherence during different stages of motor movement. One of the important hypotheses that emerged from these studies is that phase locking and coherency may represent necessary and critical properties that are generalizable between multiunit animal studies and noninvasive human EEG studies. However, before this hypothesis can be properly tested, improved spatial and temporal resolution of human scalp-derived electrophysiological measurements is necessary.

The purpose of the present paper is to present, for the first time, a method to improve the spatial and temporal resolution of human neural network dynamics using multimodal registration of PET, MRI, and EEG. The crux of the method is the computation of "instantaneous dipole coherence" to measure the dynamics of neural network coupling that precedes and follows a motor movement. Our approach is made up of three steps: (1) anatomically register MRI-referenced electrophysiological dipoles obtained during a movement task to MRI-referenced PET activation obtained during the performance of the same task (Toro *et al.*, 1994; Wang *et al.*, 1994); (2) analytically compute an EEG-derived time series for each of the MRI- and PET-validated dipoles using a pseudoinverse method (Penrose, 1955; Ben-Israel and Greville, 1974; Mosher *et al.*, 1992); and (3) compute instantaneous EEG coherence and phase from the derived

† Present address: Veterans Affairs Medical Center, Neurology Service, Bay Pines, Florida 33504.

time series in order to study the time history of the MRI- and PET-registered dipoles (Thatcher *et al.*, 1986). A specific goal of this approach is to exploit the advantages of multimodal registration of independent modalities. For example, multimodal registration of PET, MRI, and EEG allows for the anatomical localization of functional measures and, specifically, the physiological validation of dipole source activation. This conclusion is based on the assumption that the superimposition of independently derived dipole sources onto regions of PET activation is strong evidence in support of the physiological validity of the dipole sources (Toro *et al.*, 1994; Wang *et al.*, 1994). Once the anatomical locations of dipole sources are independently validated, one can apply analytical solutions to the inverse dipole source problem (Scherg, 1992; Wang *et al.*, 1992, 1993). This is a significant advantage because, without *a priori* knowledge of the location of the dipole sources, numerical analyses in which the risk of becoming trapped in local minima will always be present. Further, without *a priori* knowledge, the inverse solution of the dipole source is indeterminate; i.e., many different source locations can give rise to identical voltage distributions on the scalp (Scherg and Berg, 1991). Finally, it is hoped that this technique may yield subcentimeter spatial resolution as well as subsecond temporal resolution of the neural network switching that occurs before and after self-paced voluntary movement.

## II. Materials and Methods

### A. Subjects

A healthy right-handed 30-year-old male volunteer participated in the study.[1] The PET, MRI, and EEG protocol was approved by the clinical research subpanel of the National Institute of Neurological Disorders and Stroke, and the subject gave his written informed consent to participate in the study.

### B. Finger Movement Paradigm

The subject was comfortably seated in a recliner chair with his arms resting on the arm rests of the chair while he performed self-paced right hand index finger abductions at a rate of approximately one abduction every 4 to 5 s. The subject was asked to keep his eyes open during the task and to fixate his gaze on a target 3 m away. A total of 240 movement trials were divided into blocks of 30 movements each. A 2- to 5-min rest period occurred between each block of movements. For purposes of this study, only the first 134 trials were analyzed.

### C. EEG Recording Techniques

EEG data were recorded using 29 gold-plated electrodes applied to the scalp with collodion. The electrodes were applied to the scalp at the conventional 10–20 locations in addition to intermediate positions. Two extra channels were used to monitor EOG, and one extra bipolar channel was used to monitor EMG. The 29 scalp and 2 EOG recordings were made against a linked-ears reference. Interelectrode impedances were kept below 5 kΩ. The data were filtered using a bandpass of 0.1 to 30 Hz and digitally sampled at a rate of 100 Hz with 12-bit analog-to-digital resolution. The EMG activity from the right first dorsal interoseous (FDI) muscle was filtered with a bandpass of 100 to 1000 Hz, full wave rectified, and fed into a Schmidt trigger set to fire at EMG burst onset (Barrett *et al.*, 1985). The EEG data were collected from 3.0 s before EMG onset to 1 s after EMG onset.

### D. Dipole Source Analyses

Dipole locations were computed using the Brain Electric Source Analysis (BESA) program (Sherg and Berg, 1991) and by adjusting the spherical coordinates based on the sphere that best fit the subject's scalp (Wang *et al.*, 1993). The coordinates of the best fit dipoles were computed for a three-shell head model of 85 mm radius. Values for scalp thickness and skull thickness were assumed to be 7 and 8 mm, respectively. The cortical surface was approximated at 70 mm and the dura, at 72 mm eccentricity. The dipole moments were computed from the averaged cortical motor movement potentials in the interval of −212 to +200 ms (at which movement onset is defined at $t = 0$). Three equivalent dipole sources accounted for 95.96% of the variance of the averaged motor movement potentials. Two of the equivalent dipole sources were constrained to be bilaterally located over the motor cortical region corresponding to the hand region, and the third equivalent dipole source was unconstrained and located medially and deeper, corresponding to the supplemental motor area (SMA). The two bilateral motor cortex equivalent dipoles were derived at a latency corresponding to the peaks of the

[1] A total of four subjects in which MRI, PET, and EEG were co-registered have been studied. Because of space limitations the results of only one subject are presented in this chapter. It should be noted that the one subject is unique in the strength or magnitude of the SMA dipole. However, the temporal dynamics of dipole coherence (i.e., the latency of dipole switch onset and offset and slope values) were consistent and similar across the four subjects (Thatcher *et al.*, 1993b).

premovement MRCPs (i.e., pNS'), and the third, supplemental motor area (SMA) dipole was derived from the peak of the frontal postmovement potential (i.e., fpMp) (Toro *et al.*, 1993). The dipoles were labeled as dipole 1 for the ipsilateral motor cortex dipole, dipole 2 for the contralateral motor cortex dipole, and dipole 3 for the contralateral supplemental motor area, or SMA dipole. Details of the source analysis are given in TORO *et al.* (1993, 1994).

### E. Multimodal Registration Procedures

The subject's head surface was used as a common framework to integrate the three types of data (i.e., EEG, MRI, and PET). The multimodal registration procedure was a four-step process. First, the scalp surface and the location of each of the 29 electrodes were determined with a three-dimensional magnetic digitizer. Second, the digitized head surface was registered with the head contour obtained from the same subject's MRI. Third, the three equivalent dipole sources determined by the BESA program were mapped into the MRI coordinate system defined by the registered MRI and digitized head. Fourth, positron emission tomography (PET) images obtained from the same subject undergoing the same motor movements were then superimposed on mapped MRIs by registering the brain contours obtained from both the MRI and the PET [see Wang *et al.* (1993) for further details].

### F. Analytical Dipole Time Series Derivation

As described previously, the locations and orientations for three equivalent dipoles were obtained using the BESA spatiotemporal fitting procedure (Sherg and Berg, 1991) with respect to the movement-locked average EEG potentials. Keeping these locations and orientations fixed, time series of each dipole were analytically derived with respect to raw EEG movement-related epochs using a pseudoinverse procedure (Mosher *et al.*, 1990; Penrose, 1955).

For each time sample, the analytical pseudoinverse procedure computes the fixed-orientation dipole moments that minimize the sum (across electrodes) of squared differences between (a) the potential actually measured at an electrode and (b) the sum of theoretical dipole potentials computed for that electrode. The theoretical potential for a single dipole equals the fixed-orientation moment times a volume conduction weight, which is defined as the potential at an electrode produced by a unit dipole moment. For $M$ dipoles and $N$ scalp electrodes, an $M$-by-$N$ matrix, $W$, represents all of the volume conduction weights. That is, $W_{ij}$ represents the theoretical attenuation of unit dipole $i$ as observed at scalp location $j$ for a three-shell spherical head model (Ary *et al.*, 1981). An $M$-by-$M$ symmetric matrix, $V$, can be formed from the volume conduction weights matrix $W$ by forming the sum of cross-products across electrodes:

$$V_{ij} = \sum_{k}^{N} W_{ik} W_{jk}.$$

For each $N$-dimensional time sample, $z$, of measured potentials across scalp electrodes, an $M$-dimensional weighted vector, $y$, can be formed such that

$$y_i = \sum_{k}^{N} W_{ik} z_k.$$

Then the $M$-dimensional dipole moment time series vector $x$ is computed from the matrix equation $x = V^{-1}y$.

In actual practice, the measured scalp potentials are referenced in some fashion, whereas the theoretically computed dipole potentials are absolute values (i.e., referenced to infinity). To take this into account, it is necessary only to reference each volume conduction weight in the same way that the measured potentials are referenced. For our case of a linked A1–A2 reference, the average of the A1 and A2 volume conduction weights was subtracted from the other volume conduction weights for each dipole. This referenced weights matrix played the role of $W$ in the above computations.

### G. Instantaneous Dipole Coherence and Phase

The method of complex demodulation was used to compute instantaneous (or event-related) EEG coherence and phase for each pairing of the three derived dipole time series described above. Complex demodulation, which is characterized by a center frequency, $f$, and a half-bandwidth, $b$, produces a complex time series from a real time series, $z(t)$, in two stages (Otnes and Enochson, 1978). The first stage consists of shifting the center frequency down to zero, which results in a complex time series. The real part of this frequency-shifted time series is obtained by multiplying $z(t)$ by $\cos(2\pi ft)$, and the imaginary part is obtained by multiplying $z(t)$ by $\sin(2\pi ft)$. The second stage consists of a low-pass filter with a half-power cutoff, $b$, that is applied to both the real and the imaginary time series. The net result of this two-stage process is a complex bandpass-filtered time series having a bandpass from $f - b$ to $f + b$.

Instantaneous coherence and phase are derived from the correlation of two sets of complex time series

obtained via complex demodulation. Let $x_i(t)$ and $y_i(t)$ represent the complex values of the first and second time series, respectively, for trial epoch number $i$ and time $t$. The complex correlation of $x$ and $y$ at time $t$ is given by

$$\rho_{xy}(t) = \frac{\sum_i [X_i(t) - \langle x\rangle(t)][Y_i(t) - \langle y\rangle(t)]^*}{\sqrt{\sum_i |X_i(t) - \langle x\rangle(t)|^2 \sum_i |Y_i(t) - \langle y\rangle(t)|^2}},$$

where the asterisk denotes complex conjugation, the vertical bars denote the magnitude of a complex number, and the angular brackets denote averaging across epochs. Note that $\langle x\rangle$ and $\langle y\rangle$ are complex average potentials (i.e., event related) that are removed prior to forming the cross-products. Because the original time series were obtained by complex demodulation, the complex correlation time series is implicitly specific to the particular center frequency $f$ and bandwidth $b$. The instantaneous coherence $\gamma^2 xy$ and phase delay $\tau_{xy}$ are given by

$$\gamma^2 xy(t, f, b) = |\rho_{xy}(t)|^2$$

and

$$\tau_{xy}(t, f, b) = \frac{1}{2\pi f} \tan^{-1}\left(\frac{\mathrm{Im}[\rho_{xy}(t)]}{\mathrm{Re}[\rho_{xy}(t)]}\right),$$

where Re and Im denote the real and imaginary parts of a complex number.

Instantaneous coherence and phase for each band of interest were computed for successive 10-ms samples from −600 ms premovement to +500 ms postmovement (i.e., 60 premovement samples + 50 postmovement samples) across 134 movement-related epochs for all possible pairings of the three dipole time series. The DC offset was removed from each trial by computing a mean value for the first 200 sample points and then subtracting the mean from each sample point. The filter was initialized at the beginning of each trial and then the sample points between −3000 ms and −600 ms were used as an extended warmup period for the filter.

## III. Results

### A. Source Locations of Equivalent Dipoles

Figure 1 shows some of the waveforms elicited during the self-paced voluntary finger movement task. The Bereitschaftpotential (BP), the negative slope (NS'), the peak of the NS' (pNS'), and the frontal peak of the motor potential (fpMP) are indicated. Figure 2B shows the dipole source moments for the three equivalent sources obtained from the waveforms elicited during the task. The arrows show the latency interval over which the dipole source localizations were computed. Figure 2A consists of head diagrams showing the locations of the three sources.

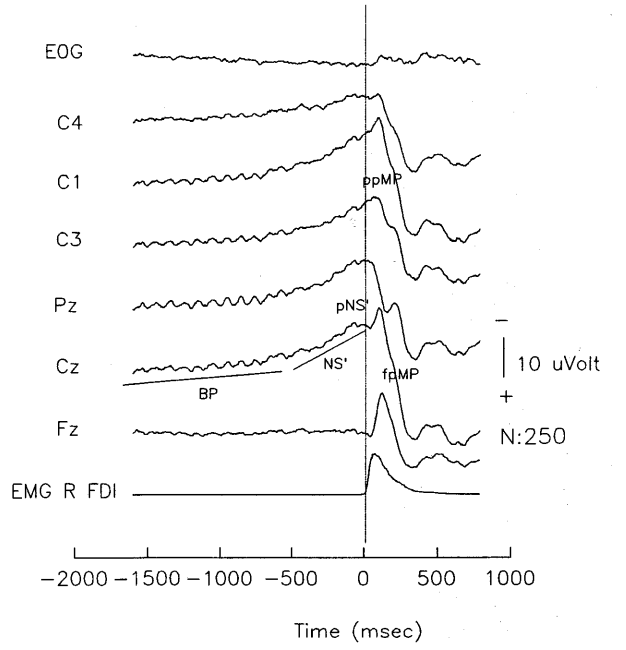


**Figure 1** Waveform morphology of the movement response cortical potential (MRCP) elicited by self-paced voluntary finger abductions in the subject of this study ($N = 250$). The BP' (Bereitschaftpotential), the negative slope (NS'), the peak of the NS' (pNS'), the parietal peak of the motor potential (ppMP), the frontal peak of the motor potential (fpMP), and the FDI EMG are shown.

### B. Multimodal Registration of Equivalent Dipoles, PET, and MRI

Plate 85 shows the location of ipsilateral motor cortex dipole 2 with respect to the registered MRI and PET. This equivalent dipole source registered within approximately 10 mm of the center of the active PET region located in the anterior bank of the ipsilateral central sulcus, near to the hand region. Plate 86 shows the location of contralateral motor cortex dipole 1. This equivalent dipole source registered within less than 3 mm of the center of the active PET region located in the anterior bank of the contralateral central sulcus, near to the hand region. Plate 87 shows the location of contralateral supplemental motor area (SMA) dipole 3. This equivalent dipole source registered within approximately 6 mm of the center of the active PET region located in the contralateral supplemental motor area.

These analyses show that there was relatively good coregistration between the location of the three equivalent dipoles and the independently obtained PET activation regions.

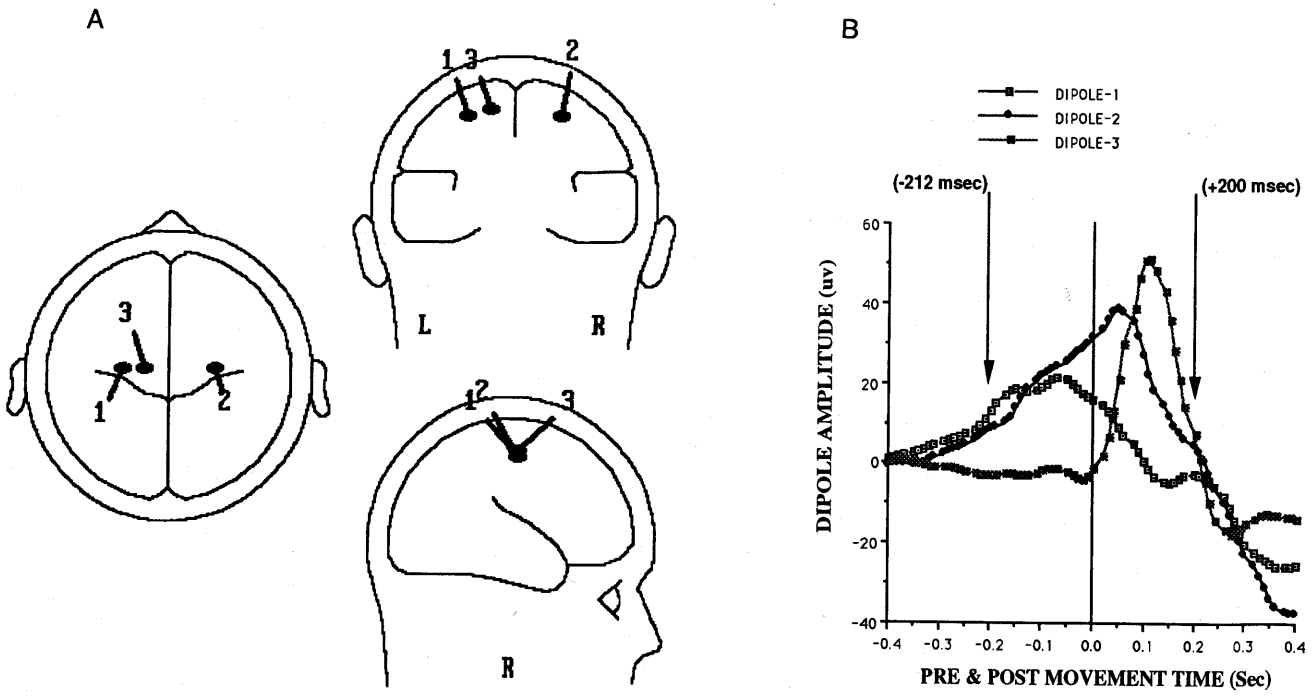


**Figure 2** Dipole source analyses of the MRCPs shown in Fig. 1. (A) The three dipole solutions over the latencies between −212 and +200 ms were calculated with two sources located on each side of the best fitting sphere (D1, ipsilateral; D2, contralateral) and one source (i.e., D3) located near the SMA. These three sources accounted for approximately 96% of the variance of the MRCP. (B) The time history of the moment magnitude of each of the three equivalent dipole sources. For further details on the methods and model, see Toro *et al.* (1993a).

## C. Instantaneous Coherence between the Pseudoinverse Derived Dipole Time Series

Figure 3 shows the results of the instantaneous coherence analyses among the time series computed for the various combinations of the three dipoles. Although changes in coherence as a function of time were noted in the center frequency range from 3 to 25 Hz, the strongest effects were seen in the $\theta$ frequency band (i.e., 4 to 7 Hz). As seen in Fig. 3A, for dipoles 1 and 2 there was a bimodal change in $\theta$ coherence between −600 and −300 ms, involving first a decline and then an increase in the magnitude of coherence. This was followed by a relatively steady-state level of coherence from −300 to 0 ms, after which there was an abrupt decrease in coherence between 0 and +50 ms postmovement. A slow recovery or increase in coherence was noted between +50 and 500 ms postmovement. In Fig. 3B, the coherence analyses for dipoles 1 and 3 were different than the analyses for dipoles 1 and 2. For example, there was a slow increase in coherence beginning at approximately −600 ms and reaching a peak at approximately −50 ms, after which there was a sudden drop in coherence just prior to movement (i.e., approximately −25 ms). During the postmovement period, coherence between dipoles 1 and 3 showed a marked increase, reaching a peak at approximately +200 ms and then declining sharply.

An inverse relationship was evident between the coherence trajectories from dipoles 1 and 3 and those from dipoles 2 and 3, as shown in Fig. 6C. That is, dipoles 2 and 3 exhibited a decrease in coherence between approximately −300 and −50 ms, after which there was a sudden increase in coherence just prior to movement (i.e., approximately −25 ms). During the postmovement period, coherence between dipoles 2 and 3 exhibited a decline followed by a marked increase at approximately +200 ms.

## D. Instantaneous Phase between the Pseudoinverse Derived Dipole Time Series

Figures 4A and 4B show an 180° phase reversal between the pseudoinverse derived time series from dipoles 1 and 2 and that from dipoles 1 and 3 during the premovement period. A rapid shift in phase from 180° to approximately 90° between dipoles 1 and 2 occurred at approximately +50 ms postmovement. Rapid shifts in phase between dipoles 1 and 3 were noted in the premovement period as well as during

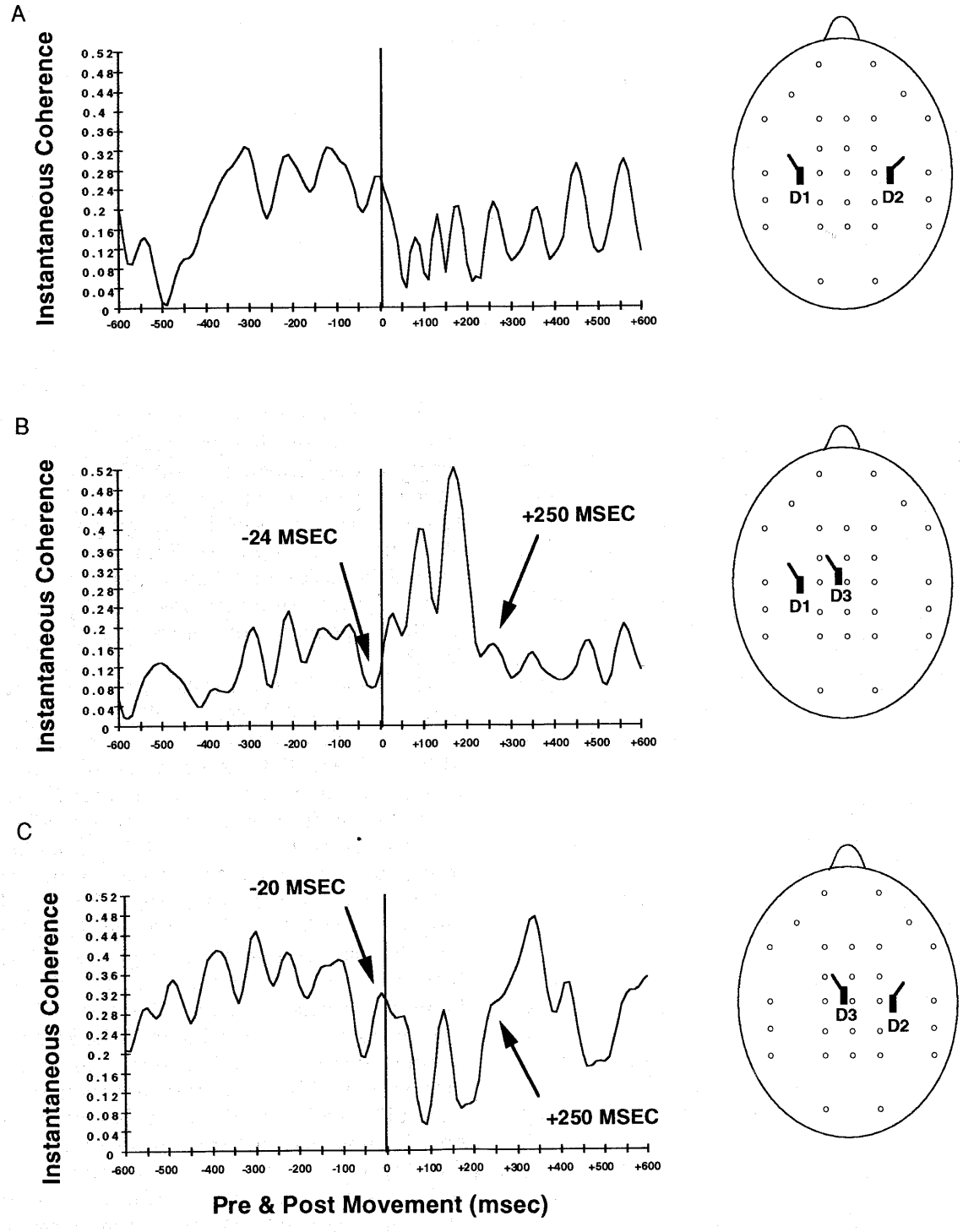


**Figure 3** Instantaneous coherence (10-ms resolution) among the pseudoinverse derived dipole time series, using a center frequency of 4.25 Hz and a bandwidth of 3.5 Hz. Instantaneous coherence on the $y$ axis is plotted against pre- and postmovement time (milliseconds) on the $x$ axis. On the right side of the figure are diagramatic representations of the location of the dipoles (see Plates 85 to 87 for exact locations). (A) Instantaneous coherence between the ipsilateral motor cortex (D2) and the contralateral motor cortex (D1). (B) Instantaneous coherence between the ipsilateral motor cortex (D2) and the contralateral supplemental motor area (SMA) (D3). (C) Instantaneous coherence between the contralateral motor cortex (D2) and the SMA (D3).

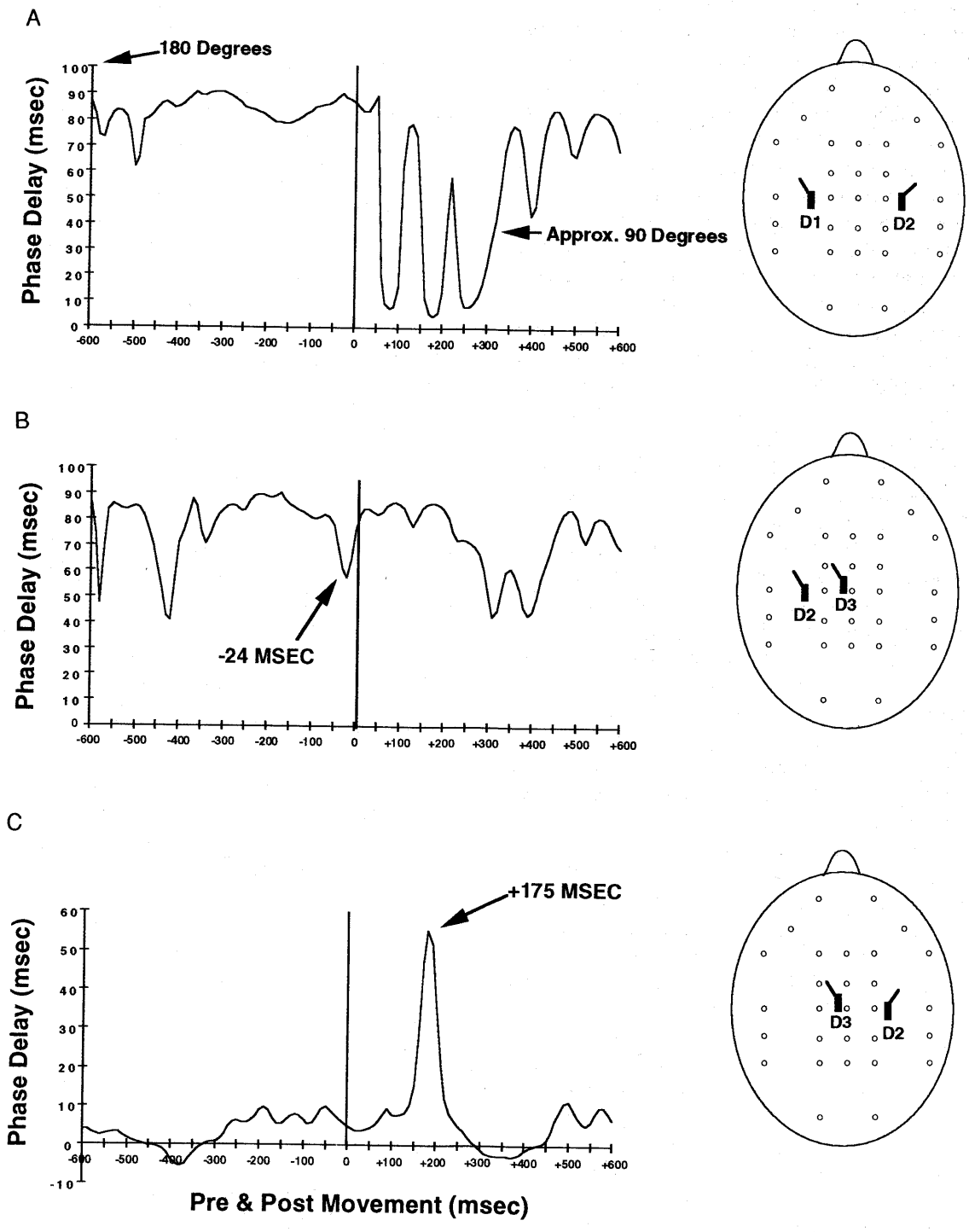


**Figure 4** Instantaneous phase delay among the pseudoinverse derived dipole time series, using a center frequency of 4.25 Hz and a bandwidth of 3.5 Hz. Phase delay (milliseconds) on the *y* axis is plotted against pre- and postmovement time (milliseconds) on the *x* axis. On the right side of the figure are diagramatic representations of the location of the dipoles (see Plates 85 to 87 for exact locations). (A) Instantaneous phase delay between the ipsilateral motor cortex (D2) and the contralateral motor cortex (D1). (B) Instantaneous phase delay between the ipsilateral motor cortex (D2) and the contralateral SMA (D3). (C) Instantaneous phase delay between the contralateral motor cortex (D1) and the contralateral SMA (D3).

the postmovement period. As seen in Fig. 4C, a distinctly different phase trajectory was observed between dipoles 2 and 3. For example, the phase relationship was near 0° during the entire premovement period with a rapid increase in phase at approximately +150 ms postmovement.

## IV. Discussion

### A. Assumptions and Limitations

In this technique, the original dipole locations and orientations were determined using averaged time-domain data. The averaging procedure in effect throws away the "background EEG" activity that was not synchronized with the motor movement. The coherence analysis, on the other hand, is a frequency domain analysis of precisely this background EEG activity (i.e., with the average removed). Thus, the two forms of analysis are complementary approaches to the same data. Because the coherence analysis was not sensitive to the time-locked average activity used to estimate the set of dipole sources, the results of this analysis are of potential physiological interest because they are not dependent upon a signal-to-noise averaging process. Instead, the analysis focuses on the magnitude and timing of "coupling" relations that precede and follow the timing of evoked potential peaks. To this extent, the "dipole coherence" analysis may be of value in the study of the subsecond neural network dynamics involved in the mediation of perception and cognition. A further advantage of this technique is that it involves an analytic and not a numeric solution to the inverse problem and thus avoids many of the pitfalls of the latter process. This stems from the use of *a priori* knowledge from multiregistration with MRI and PET (Wang *et al.*, 1993).

At the same time, the reader should be aware of the preliminary nature of this study and the assumptions relied upon. First, it is assumed that the location and orientation of the dipoles remained fixed during the analysis period. Second, it is assumed that the analytically derived dipole moments are causally related to the distribution of scalp voltages recorded at each instant of time. Third, it is assumed that the coherence and phase measures reflect the magnitude of coupling or "phase coherency" shared between the dipole moments.

### B. Face Validity of the Technique

In spite of the above noted limitations, there was considerable evidence to validate the physiological foundations of the technique. First, the anatomical accuracy of the registration of the electrophysiological dipoles with the center of the PET-activated regions varied from approximately 3 to 10 mm (see Plates 85 to 87). Second, the dipoles were located in cortical regions that are known to subserve finger movements (i.e., the anterior bank of the central sulcus and the SMA). Third, the time course of the dipole coherence events corresponded well with the time course of evoked potential (Toro *et al.*, 1993, 1994) and event-related desynchronization events (Pfurtsheller *et al.*, 1988) obtained in similar if not identical motor movement tasks. Finally, the observed rapid changes in electrophysiological coupling between distributed brain regions was similar to that observed by Gevins *et al.* (1989a, 1989b) in subjects performing a motor movement task.

### C. Competition between Dipoles

As described elsewhere, inverse relationships and 180° phase reversals in EEG coherence are believed to reflect competition between connected neural assemblies (Thatcher *et al.*, 1986, 1987, 1992). For example, for three interconnected neural assemblies, A, B, and C, increased coupling between A and B may be at the expense of coupling between A and C, B and C, or both. In the present study, increased coupling between the ipsilateral motor cortex dipole and the contralateral SMA dipole was inversely related to the magnitude of coupling between the contralateral motor cortex dipole and the contralateral SMA dipole (see Fig. 3). This is indicative of dynamic competition between the ipsilateral and contralateral motor cortex and the SMA. Another example of possible competition was seen in the coherence relationships between the ipsilateral and the contralateral motor cortex dipoles. In this case, there was a rapid decrease in coupling between the ipsilateral motor cortex (D2) and SMA (D3) immediately after motor movement (i.e., between 0 and 50 ms), which occurred simultaneously with an increase in coupling between the contralateral motor cortex dipole (D1) and the SMA dipole (D3).

### D. SMA as a Neural Network Switch Element

The SMA dipole was strongly coupled to the ipsilateral motor cortex dipole during the premovement period because these regions exhibited relatively high coherence and a zero phase lag (see Figs. 3C and 4C). In contrast, during the premovement period, the SMA dipole was weakly coupled to the contralateral motor cortex dipole with variable but near 180° phase relationships (see Fig. 3B). Evidence for an SMA role as a neural network switching element was seen by the

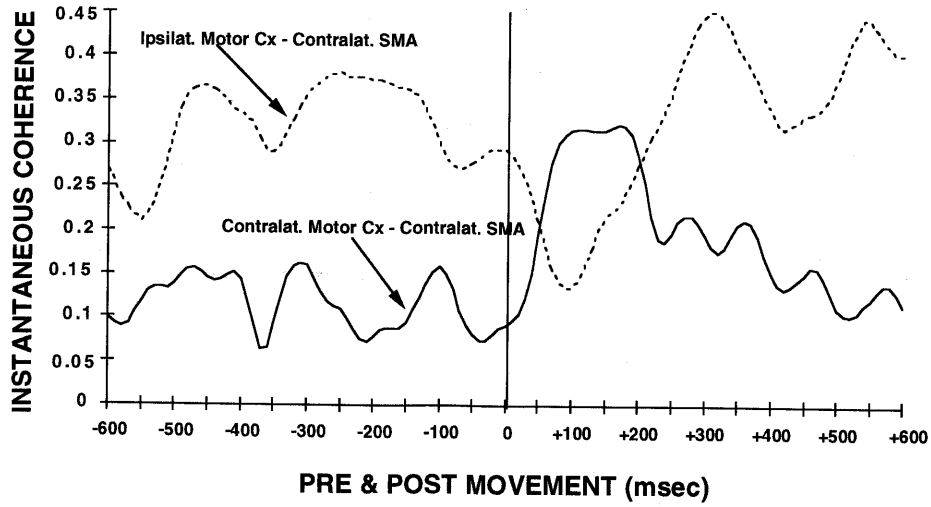


**Figure 5** Instantaneous coherence (10-ms resolution) among the pseudoinverse derived dipole time series, using a center frequency of 7 Hz and a bandwidth of 4 Hz. Coherence on the $y$ axis is plotted against pre- and postmovement time (milliseconds) on the $x$ axis. The dashed line is instantaneous coherence between the time series from the ipsilateral motor cortex and that from the contralateral SMA. The solid line is instantaneous coherence between the time series from the contralateral motor cortex and that from the contralateral SMA.

rapid (i.e., 20 to 50 ms) reversal in coherence values immediately after the motor movement (see Fig. 3). The label of the SMA dipole as a switching element is based upon the speed at which the coupling dynamics changed and the primary relationship that the SMA dipole held with respect to the other dipoles, especially the contralateral motor cortex dipole (see Figs. 3 and 5). A more detailed analysis of the dynamics of the SMA changes in coupling with respect to the ipsilateral and contralateral cortex is shown in Fig. 5. In this figure, the center frequency of the filter was set to 7 Hz and the bandwidth was limited to 4 Hz. These filter settings provided a smoother picture of the time course of coherence changes.

## E. Human Neural Network Dynamics and Zero Phase Coupling

The instantaneous coherence and phase analyses used in the present study may provide new information about the dynamics of neural interaction that occurred during the finger movement task. Three of the most significant dynamical features were (1) the presence of oscillations in coherence and phase, (2) the duration and rate of large changes in coherence and phase, and (3) the presence of zero phase locking. The presence of oscillations in dipole coherence is a function of the bandwidth of the filter; i.e., oscillations diminish as the bandwidth narrows. This suggests that the oscillations are due to periodic shifts in frequency in one or both channels. The amplitude and frequency of these oscillations may be of relevance in dynamical modeling of the coupling phenomena. We are currently conducting simulation analyses to learn more about the basis of the oscillations in the dipole coherence. The duration of the large changes in dipole coherence refers to the interval over which a relatively stable level of coherence suddenly changes to a new stable level. In the present study, this interval was approximately 50 to 100 ms (see Figs. 3 and 5). The rate of change in coherence between the pre- and the postmovement periods was estimated by derivatives to be from approximately 0.001 to 0.003 ms. Finally, zero phase locking was present only between the SMA dipole and the contralateral motor cortex dipole. As mentioned previously, this is suggestive of strong coupling between these regions, which persists even though coherence may radically change (see Figs. 3 and 4). Although more analyses must be performed on a larger number of subjects, these findings tentatively suggest that the dynamics of neural network coupling observed in multiunit studies in animals (e.g., Gray *et al.*, 1989; Eckhorn *et al.*, 1988; Murthy and Fetz, 1992) may be similar to those observed in noninvasive human EEG studies.[2]

[2] Although the PET scan is not "noninvasive," we believe that truly noninvasive techniques, such as functional MRI, provide adequate spatial resolution of regional blood flow to replace the PET [see Turner *et al.* (1993) and Turner and Jezzard (1993)].

## Acknowledgment

We acknowledge Dr. Brad Roth for his critical and constructive comments.

## References

Ary, J. P., Klein, S. A., and Fender, D. H. (1981). Location of sources of evoked scalp potentials: Corrections for skull and scalp thicknesses. *IEEE Trans. Biomed. Eng.* **37,** 447–452.

Atiya, A., and Baldi, P. (1989). Oscillations and synchronizations in neural networks: An exploration of the labeling hypothesis. *Int. J. Neural Syst.* **1**(2), 103–124.

Baldi, P., and Meir, R. (1990). Computing with arrays of coupled oscillators: An application to preattentive texture discrimination. *Neural Comput.* **2,** 458–471.

Barrett, G., Shibasaki, H., and Neshige, R. (1985). A computer-assisted method for averaging movement-related cortical potentials with respect to EMG onset. *Electroenceph. Clin. Neurophysiol.* **60,** 276–281.

Ben-Israel, A., and Greville, T. N. E. (1974). "Generalized Inverses Theory and Applications." New York: Wiley.

Bendat, J. S., and Piersol, A. G. (1980). "Engineering Applications of Correlation and Spectral Analysis." New York: Wiley.

Eckhorn, R., Bauer, R., Jordan, W., Brosch, M., Kruse, W., Munk, M., and Reitboek, H. J. (1988). Coherent oscillations: A mechanism of feature linking in the visual cortex? *Biol. Cybernetics* **60,** 121–130.

Gevins, A. S., and Bressler, S. L. (1988). Functional topography of the human brain. *In* "Functional Brain Imaging" (G. Pfurtscheller, Ed.), pp. 99–116. Berlin: Hans Huber.

Gevins, A. S., Cutillo, S. L., Bressler, S. L., Morgan, N. H., White, R. M., Illes, J., and Greer, D. S. (1989). Event-related covariances during a bimanual visuomotor task. I. Methods and analysis of stimulus- and response-locked data. *Electroenceph. Clin. Neurophysiol.* **74**(1), 58–75.

Gevins, A. S., Cutillo, S. L., Bressler, S. L., Morgan, N. H., White, R. M., Illes, J., and Greer, D. S. (1989). Event-related covariances during a bimanual visuomotor task. II. Preparation and feedback. *Electroenceph. Clin. Neurophysiol.* **74**(2), 147–160.

Gray, C. M., Konig, P., Engel, A. K., and Singer, W. (1989). Oscillatory responses in cat visual cortex exhibit inter-columnar synchronization which reflects global stimulus properties. *Nature (London)* **338,** 334–337.

Grossberg, S. (1976). Adaptive pattern classification and universal recoding. I. Parallel development and coding of neural feature detectors. *Biol. Cybernetics* **23,** 187–202.

Grossberg, S., and Somers, D. (1991). Synchronized oscillations during cooperative feature linking in a cortical model of visual perception. *Neural Networks* **4,** 453–466.

John, E. R. (1963). "Mechanisms of Memory." New York: Academic Press.

Mosher, J. C., Lewis, P. S., and Leahy, R. M. (1992). Multiple dipole modeling and localization from spatio-temporal MEG data. *IEEE Trans. Biomed. Eng.* **39**(6), 541–557.

Murthy, V. N., and Fetz, E. E. (1992). Coherent 25- to 35Hz oscillations in the sensorimotor cortex of awake behaving monkeys. *Proc. Natl. Acad. Sci. USA* **89,** 5670–5674.

Otnes, R. K., and Enochson, L. (1978). "Applied Time Series Analysis," pp. 212–215. New York: Wiley.

Penrose, R. (1955). A generalized inverse for matrices. *Proc. Cambridge Phil. Soc.* **51,** 406–413.

Pfurtscheller, G., Steffan, J., and Maresch, H. (1988). ERD mapping and functional topography: Temporal and spatial aspects. *In* "Functional Brain Imaging" (G. Pfurtscheller, Ed.), pp. 117–130. Berlin: Hans Huber.

Scherg, M., and Berg, P. (1991). Use of prior knowledge in brain electromagnetic source analysis. *Brain Topogr.* **4,** 143–150.

Scherg, M. (1992). Functional imaging and localization of electromagnetic brain activity. *Brain Topogr.* **5**(2), 103–111.

Talairach, J., and Tournoux, P. (1988). "Co-Planar Stereotaxic Atlas of the Human Brain." New York: Thieme Medical.

Thatcher, R. W., and John, E. R. (1977). "Functional Neuroscience: Foundations of Cognitive Processes." New Jersey: Erlbaum.

Thatcher, R W., Krause, P., and Hrybyk, M. (1986). Corticocortical association fibers and EEG coherence: A two compartmental model. *Electroenceph. Clin. Neurophysiol.* **64,** 123–143.

Thatcher, R. W., Walker, R. A., and Giudice, S. (1987). Human cerebral hemispheres develop at different rates and ages. *Science* **236,** 1110–1113.

Thatcher, R. W. (1992). Cyclic cortical reorganization during early childhood. *Brain Cog.* **20,** 24–50.

Thatcher, R. W., Toro, C., and Hallett, M. (1993a). Neural network switching during voluntary finger movements. *In* "International Federation of Clinical Electroencephalography, Vancouver, B.C." [Abstr.]

Thatcher, R. W., Toro, C., Pflieger, M. E., and Hallett, M. (1993b). Multimodal registration of EEG, PET and MRI: Analyses of Neural Network Switching. *Proceedings of Society of Magnetic Resonance in Medicine: Functional MRI of the Brain.* Arlington, VA, June 17–19, pp. 171–181.

Toro, C., Matsumoto, J., Deuschl, G., Roth, B. J., and Hallett, M. (1993a). Source analysis of scalp-recorded movement-related electrical potentials. *Electroenceph. Clin. Neurophysiol.* **86,** 167–175.

Toro, C., Wang, B., Zeffiro, T. A., Thatcher, R. W., and Hallett, M. (1994). Movement related cortical potentials: Source analysis and PET/MRI correlation. *In* "Functional Neuroimaging: Technical Foundations" (R. W. Thatcher, M. Hallett, T. Zeffiro, E. R. John, and M. Huerta, Eds.). Orlando, FL: Academic Press.

Turner, R., Jezzard, P., Wen, H., Kwong, K. K., Le Bihan, D., Zeffiro, T., and Balaban, R. S. (1993). Functional mapping of the human visual cortex at 4 and 1.5 tesla using deoxygenation contrast EPI. *Magn. Reson. Magazine* **29,** 277–279.

Turner, R., and Jezzard, P. (1993). MR studies of brain functional activation using echo-planar imaging. *In* "Functional Neuroimaging: Technical Foundations" (R. W. Thatcher, M. Hallett, T. Zeffiro, E. R. John, and M. Huerta, Eds.). Orlando, FL: Academic Press.

von der Malsburg, C., and Schneider, W. (1986). A neural cocktail-party processor. *Biol. Cybernetics* **54,** 29–40.

Wang, B., Toro, C., Wasserman, E. M., Zeffiro, T. A., Thatcher, R. W., and Hallett, M. (1994). Multimodal integration of electrophysiological data and brain images: EEG, MEG, TMS, MRI, and PET. *In* "Functional Neuroimaging: Technical Foundations" (R. W. Thatcher, M. Hallett, T. Zeffiro, E. R. John, and M. Huerta, Eds.). Orlando, FL: Academic Press.

Wang, J., Williamson, S. J., and Kaufman, L. (1992). Magnetic source images determined by a lead-field analysis: The unique minimum-norm least-squares estimation. *IEEE. Trans. Biol. Med.* **39**(7), 665–675.

Wang, J., Kaufman, L, and Williamson, S. J. (1993b). Imaging regional changes in the spontaneous activity of the brain: An extension of the minimum-norm least-squares estimate. *Electroenceph. Clin. Neurophysiol.* **86,** 36–50.

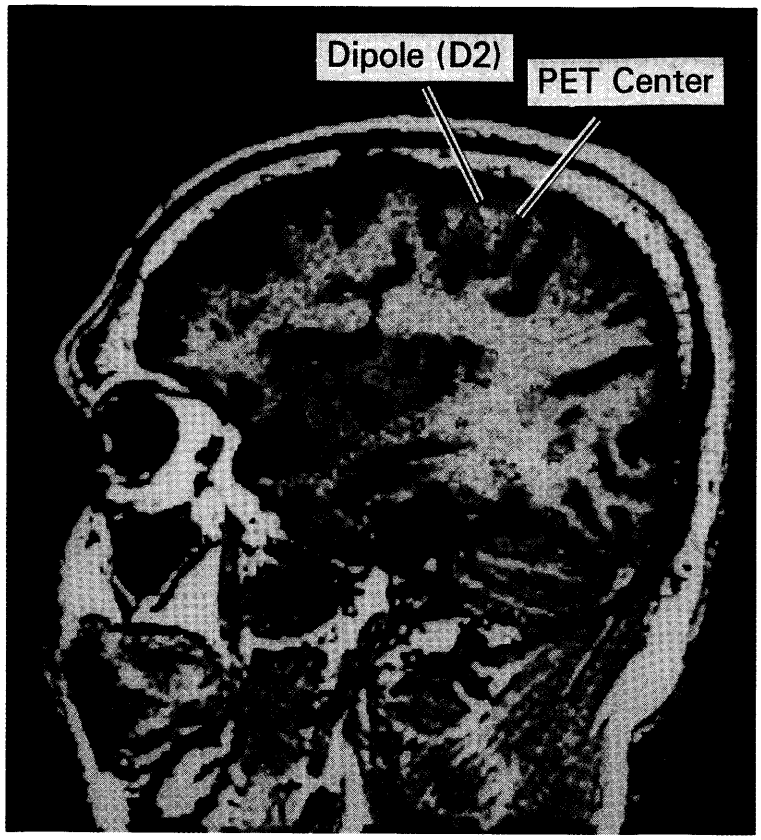


**Plate 85** Multimodal sagittal image of the ipsilateral right hemisphere (sagittal slice No. 74). The rCBF PET image registered with the corresponding sagittal MRI was obtained after averaging three images obtained during the execution of self-paced right index finger movements after the injection of $H_2O^{15}$ and subtraction from averaged rest scans. The location of source 2 (i.e., D2; see Fig. 2) in the spherical head model, in the same subject executing the same task, has been projected into the PET and MRI images (open cross) after the appropriate coordinate transformations and rotations. See Wang *et al.* (1993a) for more details of the technique. Both the dipole source and the active PET region are located near the ipsilateral hand region in the anterior bank of the central sulcus. The distance between the dipole source location (left arrow) and the center of the active PET region (right arrow) is approximately 10 mm. The Talairach and Tournoux (1988) atlas coordinates of the registered PET and dipole source 2 are approximately c, 3, and $E_2$ in the right hemisphere. (Coordinates *x*, *y*, *z* are +1.4 cm horizontal, +4.1 cm medial-lateral, and +5.0 cm top to bottom.)


**Plate 86** Multimodal sagittal image of the contralateral left hemisphere (sagittal slice No. 36). The rCBF PET image registered with the corresponding sagittal MRI was obtained after averaging three images obtained during the execution of self-paced right index finger movements after the injection of $H_2O^{15}$ and subtraction from averaged rest scans. The location of source 1 (i.e., D1; see Fig. 2) in the spherical head model, in the same subject executing the same task, has been projected into the PET and MRI images (open cross) after the appropriate coordinate transformations and rotations. See Chapter 25 for more details of the technique. Both the dipole source and the active PET region are located near the hand region in the anterior bank of the central sulcus. The distance between the dipole source location (left arrow) and the center of the active PET region (right arrow) is less than 3 mm. The Talairach and Tournoux (1988) atlas coordinates of the registered PET and dipole source 1 are approximately c, 3, and $E_2$ in the left hemisphere. (Coordinates *x*, *y*, *z* are +1.4 cm horizontal, +4.1 cm medial-lateral, and +5.0 cm top to bottom.)

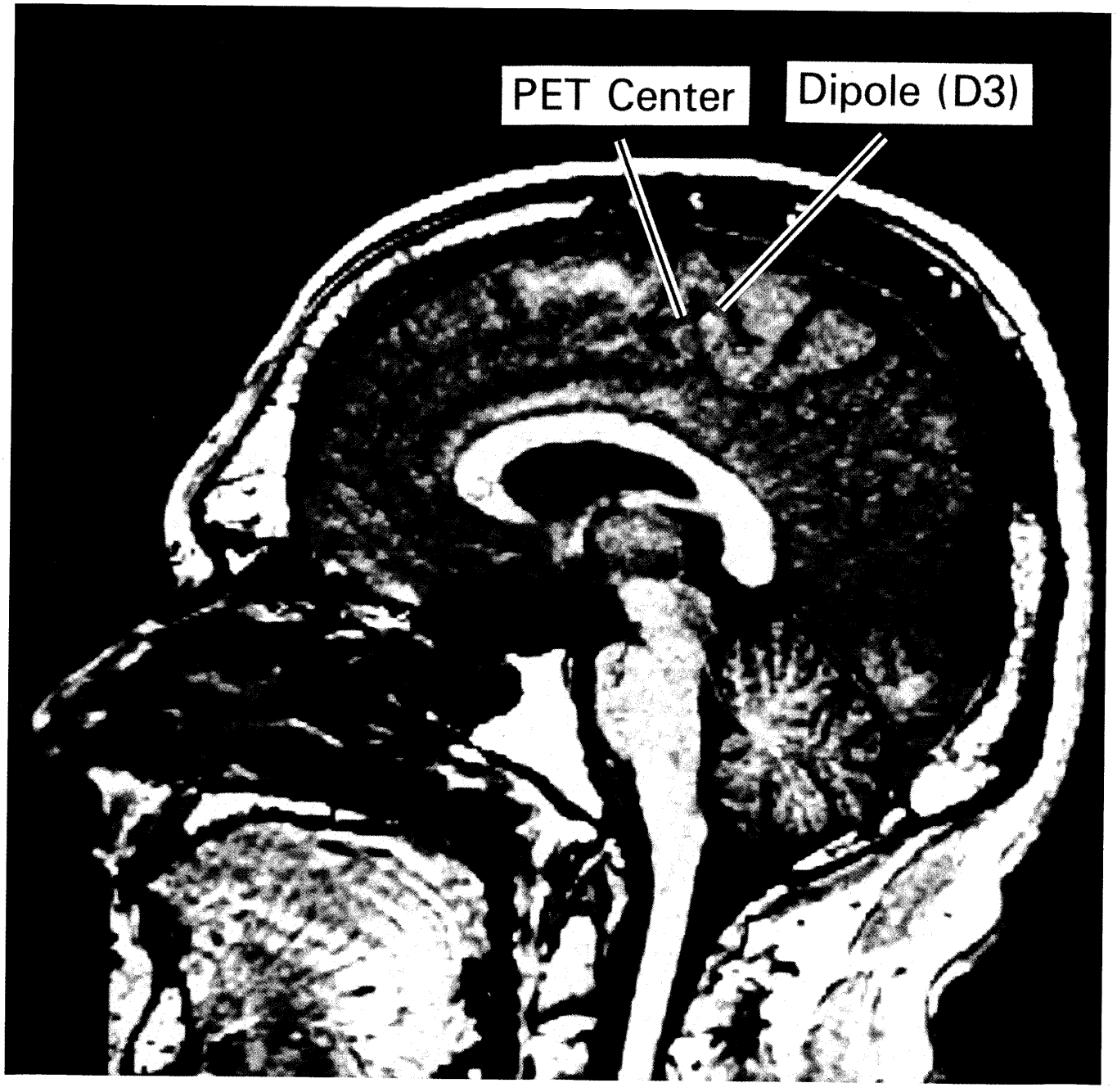


**Plate 87** Multimodal sagittal image of the contralateral left hemisphere (sagittal slice No. 51). The rCBF PET image registered with the corresponding sagittal MRI was obtained after averaging three images obtained during the execution of self-paced right index finger movements after the injection of $H_2O^{15}$ and subtraction from averaged rest scans. The location of source 3 (i.e., D3; see Fig. 2) in the spherical head model, in the same subject executing the same task, has been projected into the PET and MRI images (open cross) after the appropriate coordinate transformations and rotations. See Chapter 25 for more details of the technique. Both the dipole source and the active PET region are located in the anterior bank of the supplemental motor cortical region. The distance between the dipole source location (left arrow) and the center of the active PET region (right arrow) is approximately 6 mm. The Talairach and Tournoux (1988) atlas coordinates of the registered PET and dipole source 3 are approximately a, 3-4, and $E_1$ in the left hemisphere. (Coordinates $x, y, z$ are +0.4 cm horizontal, +0.5 cm medial-lateral, and +4.6 cm top to bottom.)